

UC Irvine

UC Irvine Previously Published Works

Title

2-Aminopyridines with a Truncated Side Chain To Improve Human Neuronal Nitric Oxide Synthase Inhibitory Potency and Selectivity.

Permalink

<https://escholarship.org/uc/item/8wb4b6jc>

Journal

Journal of Medicinal Chemistry, 58(14)

Authors

Tang, Wei

Martásek, Pavel

Roman, Linda

et al.

Publication Date

2015-07-23

DOI

10.1021/acs.jmedchem.5b00573

Peer reviewed



HHS Public Access

Author manuscript

J Med Chem. Author manuscript; available in PMC 2016 July 23.

Published in final edited form as:

J Med Chem. 2015 July 23; 58(14): 5548–5560. doi:10.1021/acs.jmedchem.5b00573.

2-Aminopyridines with a Truncated Side Chain to Improve Human Neuronal Nitric Oxide Synthase Inhibitory Potency and Selectivity

Soosung Kang^{†,¶}, Huiying Li[‡], Wei Tang[†], Pavel Martísek[§], Linda J. Roman[§], Thomas L. Poulos^{*,‡}, and Richard B. Silverman^{*,†}

[†]Department of Chemistry, Department of Molecular Biosciences, Chemistry of Life Processes Institute, Center for Molecular Innovation and Drug Discovery, Northwestern University, 2145 Sheridan Road, Evanston, Illinois 60208-3113, United States

[‡]Departments of Molecular Biology and Biochemistry, Pharmaceutical Sciences, and Chemistry, University of California, Irvine, California 92697-3900, United States

[§]Department of Biochemistry, University of Texas Health Science Center, San Antonio, Texas 78384-7760, United States

[¶]New Drug Development Center, DGMIF, 80 Cheombok-ro, Dae-gu, Korea

Abstract

We have analyzed a recently obtained crystal structure of human neuronal nitric oxide synthase (nNOS), then designed and synthesized several 2-aminopyridine derivatives containing a truncated side chain to avoid the hydrophobic pocket that differentiates human and rat nNOS in an attempt to explore alternative binding poses along the substrate access channel of human nNOS.

Introduction of an *N*-methylethane-1,2-diamine side chain and conformational constraints such as benzonitrile and pyridine as the middle aromatic linker were sufficient to increase human and rat nNOS binding affinity and inducible and endothelial NOS selectivity. We found that **14b** is a potent inhibitor; the binding modes with human and rat nNOS are unexpected, inducing side chain rotamer changes in Gln478 (rat) at the top of the active site. Compound **19c** exhibits K_i values of 24 and 55 nM for rat and human nNOS, respectively, with 153-fold iNOS and 1040-fold eNOS selectivity. **19c** has 18% oral bioavailability.

Keywords

nitric oxide synthase; neurodegenerative diseases; human nNOS; selective inhibition

*Corresponding Author Richard B. Silverman, Department of Chemistry, Northwestern University, Evanston, Illinois 60208-3113; Phone: (847) 491-5653; Fax (847) 491-7713; Agman@chem.northwestern.edu. *Corresponding Author Thomas L. Poulos, Departments of Molecular Biology and Biochemistry, Pharmaceutical Sciences, and Chemistry, University of California, Irvine, California 92697-3900; Phone: (949) 824-7020; Fax: (949) 824-3280; poulos@uci.edu..

Supporting Information. Crystallographic data collection, structure refinement statistics, and LC-MS/MS conditions. This material is available free of charge via the Internet at <http://pubs.acs.org>.

PDB codes for structures reported here: nNOS-**10a**, 4UGZ; nNOS-**14a**, 4UH0; nNOS-**14b**, 4UH1; nNOS-**19a**, 4UH2; nNOS-**19b**, 4UH3; nNOS-**19c**, 4UH4; HnNOS-**14b**, 4UH5; HnNOS-**19c**, 4UH6; eNOS-**10a**, 4UH7; eNOS-**14b**, 4UH8; eNOS-**19b**, 4UH9; eNOS-**19c**, 4UHA.

INTRODUCTION

Production of the unique biological messenger, nitric oxide (NO), in mammals by nitric oxide synthases (NOSs) is essential for diverse physiological processes, such as angiogenesis, neurotransmission, immune response, insulin secretion, and modulation of vascular tone.^{1, 2} NOSs use L-arginine, molecular oxygen, NADPH, and other cofactors, such as flavin adenine dinucleotide (FAD), flavin mononucleotide (FMN), heme, and tetrahydrobiopterin (H₄B) to synthesize NO in three principal isoforms: neuronal NOS (nNOS), endothelial NOS (eNOS), and inducible NOS (iNOS).³ Each NOS isoform is expressed in different tissues or cell types, and the NO production from each isoform has a distinct regulatory role.⁴ Overproduction of NO, however, is involved in diverse diseases; excess NO by iNOS is connected with septic shock,⁵ inflammatory, and immunologically mediated diseases, as well as complications from diabetes.⁶ Excess NO by nNOS in the central nervous system has been implicated in the pathogenesis of diverse neuronal disorders, such as Alzheimer's disease,⁷ Parkinson's disease,⁸ and ALS.⁹ Although inhibition of nNOS has the potential for control of diverse neurodegenerative diseases, selective inhibition is essential to minimize any unwanted side effects^{10, 11} because of the involvement of NO signaling in fundamental physiological functions.

Although many nNOS inhibitors have been reported by others (Figure 1, **1-2**)^{12,13,14} and our research group (Figure 1, **3-6**),^{15,16,17,18} development of selective inhibitors of nNOS against iNOS and eNOS is still a challenge because the active sites of NOSs are nearly identical among all three isoforms.¹⁹ For historical reasons, we have been using rat nNOS and bovine eNOS for crystallographic studies. In these studies, we concluded that a guanidine isostere such as 2-aminopyridine²⁰ and 2-aminoquinoline, or an iron-binding motif such as 2-imidazolylpyrimidine, is essential to achieve the NOS active site recognition via hydrogen bonds with an active site glutamate residue or by a direct ligation bond to the heme iron. In addition, the 3-fluorophenethyl moiety of **4-6** is necessary for additional selectivity by occupying a peripheral hydrophobic pocket along the substrate access channel.²¹ We have also observed a unique nNOS selective induced-fit conformational change²² in which Tyr706 of rat nNOS is more readily rotated out to adopt an out-rotamer conformation, while the corresponding Tyr477 in bovine eNOS remained in an in-rotamer position. The out-rotamer conformation provides better H-bonding (salt-bridge) between the protein (heme propionates) and inhibitors, thus increasing nNOS potency and selectivity over eNOS.

The design of rat nNOS-selective inhibitors is very important for success in preclinical studies, leading to clinical studies. However, because drugs are typically designed for human disease treatment, it is imperative to attain high potency for human targets. If drug candidates are excellent human target inhibitors, but weak lower animal target inhibitors, they will never have acceptable efficacy to advance to clinical trials. Likewise, if they are excellent lower animal target inhibitors, but weak human target inhibitors, they will fail in clinical trials. Therefore, it is imperative to identify target inhibitors that have comparable and high potency for both lower animal and human targets.

Because the primary sequence of rat nNOS is almost identical (> 93%) to human nNOS and the nNOS active site for each mammalian species is highly conserved, an inhibitor binding to rat nNOS was thought to reflect the binding behaviors to human nNOS. However, we have observed that compounds that were developed based on the rat nNOS crystal structure often displayed 5- to 10-fold weaker inhibitory activity toward human nNOS. Recently, we succeeded in obtaining a crystal structure of human nNOS.²³ An active site overlay of human nNOS with rat nNOS (Figure 2B) showed that the active site structures of the two mammalian nNOSs are identical, and the only difference is in the peripheral pocket, where Leu337 of rat nNOS is replaced by a histidine (His342) in human nNOS (Figure 2C). The human peripheral pocket containing a histidine is relatively more narrow and more polar; consequently, it prefers inhibitors to have a less bulky and more hydrophilic tail. That may explain why our previous nNOS selective compounds fit well into the rat NOS Leu337 hydrophobic pocket but displayed decreased potency against human nNOS.

Compounds **1** and **2**, having an amidine^{13-15,21} and a methylamine tail with a tetrahydroquinoline or indoline core, recently reported by other research groups, display good potency toward human nNOS.^{12,13,14} Although 3-dimensional structural information of these compounds with nNOS were not reported, our previous crystallographic experience²⁴ indicates that the thiophene-carboximidamide moiety should occupy the substrate binding pocket over the heme, and the tetrahydroquinoline or indole core should share the binding site with the middle aromatic ring of **3** near the C and D ring propionates. The *N*-methyl substituted alkylamine chains from the core should improve the selectivity and potency by interacting with residues peripheral to the active site.

We have recently reported a double-headed aminopyridine compound (**3**, Figure 1) that uses its methylamine group to interact with both heme propionate A and the H₄B, thereby displacing a water molecule. Although the same binding mode was maintained in both nNOS and eNOS, different electrostatic environments in the active site of nNOS and eNOS resulted in distinct isoform binding affinity, leading to good isoform selectivity.¹⁶

On the basis of these observations we attempted to design new human nNOS selective and potent compounds via hybridization of the potent molecular fragment of compound **3** (the 2-aminopyridine attached to an aromatic ring) and the human nNOS adaptable alkylamine fragment from compound **1**, with the goal of displacing the H₄B conserved water molecule. It is possible that the alkylamine fragment of compound **1** corresponds to the alkylamine tail of compound **3**. To avoid the Leu337/His342 difference between rat nNOS and human nNOS in the hydrophobic cleft one of the aromatic heads of compound **3** was removed and substituted with an alkylamine chain. The other aminopyridine ring of **3** was retained as an isostere of guanidine, and the middle aromatic linker and *N*¹ or *N*²-methyl substituted ethylenediamine tail were varied. Because substitution on the middle aromatic ring provided bioactivity during our previous exploration with symmetric molecules,²⁵ the middle aromatic linker was substituted with cyano, fluorine, trifluoromethyl, and substituted by pyridine. The molecules in Figure 3, having a truncated side chain and various substitutions of the middle aromatic ring, were synthesized and their inhibitory potencies were determined *in vitro*. Crystal structures of the promising compounds were obtained using either rat nNOS or human nNOS, as well as bovine eNOS. The primary aim of this study is

to generate a modified scaffold from our previous aminopyridine derivatives for improved potency against human nNOS and investigate its influence on the binding mode. This should build a foundation for further design of potent, selective, and bioavailable inhibitors for human nNOS.

Results and Discussion

Chemistry

All compounds described here were prepared from various aryl bromides in three steps: a coupling reaction, a Buchwald-Hartwig amination, and pyrrole deprotection (Schemes 1-3). The coupling reaction of an aryl bromide (**8**, **11a-b**, **15a-c**) and lithiated pyrrolyl-4,6-dimethylpyridine, which was prepared by addition of BuLi to pyrrolyl-4,6-dimethylpyridine (**7**), gave an arylolethylpyridine intermediate (**9**, **12a-b**, **16a-c**). One bromine atom in dibromo intermediate **16c** was converted to the nitrile (**17**) by microwave assisted cyanation with CuCN. Next, Buchwald-Hartwig amination²⁶ of **9**, **12a-b**, **16a-b**, and **17** with *N,N'*-dimethyldiamine was performed using a catalytic amount of Pd₂(dba)₃ and DavePhos. Sterically hindered ligand DavePhos was more efficient than BINAP and DPPF at coupling with a secondary amine. Finally, the pyrrole protecting group on the aminopyridine was removed from **9**, **13a-b**, and **18a-c** by microwave-aided hydrolysis to give final compounds **10a-d**, **14a-b**, and **19a-c** in good yields. Because the Buchwald-Hartwig products of **9a-d** produced mainly the desired amine intermediates, those intermediates were passed through a 2-cm silica gel pad and used in the next deprotection step without further purification or characterization. Purification of these final polar compounds was performed by flash column chromatography using C-18 prepacked cartridges.

Bioactivity of **10a-d**, **14a-b**, and **19a-c**

The oxyhemoglobin NO assays were performed with purified NOSs to measure K_i values of the synthesized compounds, as previously described.^{27,28} Compounds **10a-d** were found to have good potency for rat nNOS and modest isoform selectivity toward bovine eNOS and murine iNOS. Compounds **14a-b** and **19a-c**, having an *N,N'*-dimethylethylenediamine tail and a modified middle aromatic ring, were found to have good binding affinity to both rat and human nNOS as well as good selectivity (238-1040 of e/n, 122-166 of i/n). Inhibitory constants (K_i) for all of the synthesized molecules are shown in Table 1.

Structure-activity relationship studies—The *N*¹,*N*²-dimethylethane-1,2-diamine side chain was chosen as the tail in the initial study after consideration that Buchwald amination with a symmetric diamine provides a better synthetic pathway than with asymmetric diamines. The inhibitory activities shown in Table 1 indicate that the terminal amine (*N*²) has a better binding affinity when it is a primary amine (**10c**). Methylation of *N*² to make it a secondary (**10a**) or a tertiary (**10b**) amine results in a 2-3 fold drop in potency toward nNOS. Methylation of *N*¹ seems to have less of an effect on potency. Compound **10d**, which has a one-carbon longer side chain compared to **10c**, had a slightly lower binding affinity toward nNOS with poor selectivity over iNOS and eNOS. Although **10d** also bears a primary amine like **10c**, its one methylene longer linker pushes the amine away from a suitable position to

make a hydrogen bond with heme propionate D, and, therefore, is the weakest binder among the four inhibitors (Table 1).

Crystal structures of **10a** bound to nNOS and eNOS are shown in Figure 4. In both structures, **10a** uses its aminopyridine group to make hydrogen bonds with the active site Glu residue, Glu592 in nNOS or Glu363 in eNOS. The middle phenyl ring presses against the heme propionate from pyrrole ring D (propionate D), but the N¹ atom is only at van der Waals distance from the propionate. The three atoms in the tail of **10a** are partially disordered in both nNOS and eNOS structures. In eNOS, the N² amine approaches heme propionate D close enough to make a hydrogen bond, but in nNOS the density for the tail is too poor to support a clear model. Nevertheless, the structural features found here explain why N¹ methylation does not affect the potency while the basicity of the N² amine contributes to binding. The primary N² amine in **10c** is expected to make the tail more stable through a better hydrogen bond with heme propionate D.

Compounds **14a** and **14b**, having a pyridine as the aromatic linker, improved the potency by 3- to 6-fold as well as improved selectivity against iNOS and eNOS. In addition, these two molecules show excellent potency (64 and 59 nM) for human nNOS. The binding mode of **14a** closely resembles that of **10a**, as shown in Figure 5A, where the middle pyridine presses against heme propionate D but neither the ring nitrogen atom nor the N¹ amine is in hydrogen bonding distance to heme propionates. The tail N² secondary amine is partially disordered but is highly likely making a hydrogen bond with heme propionate D. The only difference in **14b** from **14a** is the position of the nitrogen atom in the middle pyridine ring, changing from the *ortho*-position relative to the other two substituents in **14a** to the *meta*-position in **14b**. This change brings in a binding mode to nNOS that is unprecedented with any other NOS inhibitors we have investigated. As seen in Figure 5B, while the aminopyridine of **14b** is still anchored by the Glu592 side chain, its middle pyridine ring takes an entirely different turn, going upward and making a hydrogen bond with Tyr562. For this to happen, the Gln478 side chain has to adopt an alternate rotamer position. With regard to the diamine tail, only the N¹ amine position is well defined, but the positions of the last three atoms are ambiguous with weaker density. In one subunit, the N² amino group can displace the water molecule that usually bridges between H₄B and heme propionate A, but in the other subunit, the water molecule seems to be retained, and the tail of **14b** steers away from it, which represents two possible tail positions.

We have also determined the crystal structure of human nNOS with **14b** bound (Figure 6A). The binding mode of **14b** to human nNOS is essentially identical to that observed in rat nNOS. The only difference is that the diamine tail of **14b** has displaced the bridging water molecule between the H₄B and heme propionate A in human nNOS without any uncertainty. It is interesting that this upward binding mode of **14b** found in nNOS does not repeat in the eNOS structure (Figure 6B). The middle pyridine of **14b** in eNOS sits on top of two heme propionates with only van der Waals contacts, while the aminopyridine ring is anchored to Glu363. The positions of the last three atoms in the tail are less certain. Overall, the upward binding mode of **14b** seen in nNOS exhibits more favorable hydrogen bonding interactions than the “straight” binding mode in eNOS, even though it involves a rotamer change of Gln478 (Figure 6C). The different binding preference for **14b** provides a structural basis for

the observed 759-fold selectivity for nNOS over eNOS. However, why **14b** chooses two different binding modes in two NOS isoforms is not apparent, considering the residues making direct contacts with **14b** are conserved.

The binding mode variations observed with **14a** and **14b** encouraged us to further explore the properties of the middle aromatic ring. Compounds **19a**, **19b**, and **19c** have a trifluoromethylphenyl ring, a fluorophenyl ring, or a benzonitrile, respectively, as the aromatic linker between the aminopyridine head and the ethylenediamine tail. The structure of **19a** bound to rat nNOS (Figure 7A) reveals a highly disordered trifluoromethyl phenyl ring, which likely fits into the open space defined by Glu592, Arg596, Asp597, and heme propionate A. There is no specific enzyme-inhibitor interaction other than more loose van der Waals contacts. The position of the tail amine also is not certain, but it may be in the vicinity of Asn569. The trifluoromethylphenyl ring is apparently too bulky to have a good fit with any other orientations in the nNOS active site. Although the diamine tail of **19b** is partially disordered, the smaller fluorophenyl ring in **19b** is well resolved. The fluorine closely interacts with heme pyrrole ring D at a distance shorter than 3.0 Å (Figure 7B). These improved interactions very likely account for the 2-fold higher potency of **19b** relative to **19a**. The secondary N² amino group can interact with either heme propionate D or the bridging water molecule between the H₄B and heme propionate A. Although **19b** was found to have a 900-fold selectivity for rat nNOS over bovine eNOS, the binding mode observed in the eNOS structure (Figure 7C) is almost identical to that seen in nNOS (Figure 7B). As we have discussed in the past¹⁶ the electrostatic environments of nNOS and eNOS are sufficiently different, mainly because of a one-residue variation (Asp597 in nNOS vs. Asn368 in eNOS), that they can have distinct impacts on the inhibitor binding affinity, even for those with identical binding conformations.

When the middle aromatic linker was changed to a benzonitrile, as in **19c**, the inhibitor was the most potent and selective in this series with a K_i of 24 nM and 1040-fold selectivity for nNOS over eNOS (Table 1). Despite the fact that the N¹,N²-dimethylethane-1,2-diamine side chain of **19c** does not reach the His342 pocket (Leu337 in rat nNOS), which was originally thought to be a good alkylamine target for human nNOS potency and selectivity, **19c** has good binding affinity toward human nNOS (K_i of 55 nM). For the bulky benzonitrile ring of **19c** to have enough room (Figure 8A), the middle aromatic ring rises upward from the plane of the aminopyridine ring so that the cyano nitrogen points toward Ser477, although without a strong hydrogen bond. The tail N² amino group can easily reach between the ketone oxygen atom of the H₄B and heme propionate A, displacing the water molecule there. The same binding mode of **19c** is conserved in human nNOS (Figure 8B), leading to good potency (54 nM) for human nNOS as well as rat nNOS. The occupation of the water molecule site with an amino group has been implicated in the gain of nNOS over eNOS inhibitor selectivity with other aminopyridine compounds.¹⁶ Here we observed a similar pattern for **19c** because the tail N² amino group of **19c** in the eNOS structure does not directly displace the water molecule; rather, the water molecule is repelled by a methylene in the diamine tail (Figure 8C). The different diamine tail position in eNOS results from a different position of the benzonitrile ring. The superimposition of the eNOS and nNOS structures with **19c** bound illustrates this distinction (Figure 8D). The middle

aromatic ring in eNOS is packed directly against heme propionates (low-position), while in nNOS it is farther away (high-position). The cyano nitrogen atom of **19c** in eNOS makes a hydrogen bond with Asn340, not with Ser248 (equivalent to Ser477 in nNOS).

Finally, the plasma pharmacokinetics and brain distribution of **19c** in male BALB/c mice following a single intravenous and oral dose administration were carried out. Table 2 presents the pharmacokinetic parameters for **19c**. At a single intravenous administration of **19c** to male BALB/c mice at a 2 mg/kg dose, the compound showed high plasma clearance (184 mL/min/kg, the normal liver blood flow in mice = 90 mL/min/kg) with an elimination half-life of 1.1 h. Following a single oral administration of **19c** to male BALB/c mice at a dose of 10 mg/kg, plasma and brain concentrations were quantifiable up to 24 h with a T_{max} of 0.25 h in plasma. Compound **19c** was slowly cleared from brain (clearance = 21 mL/min/kg) with appreciable brain concentrations detectable up to 24 h, and concentrations were approximately flat from 2 to 24 h. Compound **19c** has a modest oral bioavailability of 18%.

Conclusions

The only structural difference that may affect the inhibitor binding between human and rat nNOS is in a peripheral binding pocket along the substrate access channel, His342 of human nNOS, which is larger and more polar than Leu337 in rat nNOS. In this work, we have designed 2-aminopyridine compounds with a middle aromatic ring and a truncated tail so that none of the diamine tails of these compounds was long enough to reach the peripheral hydrophobic pocket, which thereby allowed for less differentiation between rat and human nNOS, resulting in binding constants that were comparable for rat and human nNOS. The introduction of substituents, such as a nitrile (**19c**) or fluorine atom (**19b**) in the middle aromatic linker was sufficient to increase nNOS binding affinity and iNOS/eNOS selectivity. The binding modes of **14b** were unexpected, which induced side chain rotamer changes in Gln478 at the top of the active site; however, a different mode was observed in eNOS. Some good inhibitors in this series exhibit low nanomolar binding affinity to both rat and human nNOS, and >100-fold and >200-fold selectivity over iNOS and eNOS, respectively. Specifically **19c** has a K_i of 24 and 55 nM for rat and human nNOS, respectively, with 153-fold (iNOS) and 1040-fold (eNOS) selectivity, and this compound has 18% oral bioavailability. As designed, no binding mode difference was found between rat and human nNOS for this series of inhibitors, because the side chain does not reach the peripheral pocket where His342 in human nNOS replaces Leu337 in rat nNOS. Further exploration of this site to improve the affinity to human nNOS is underway.

Experimental section

Materials, synthetic methods, and molecular characterization

All starting materials were purchased from Sigma-Aldrich and Matrix Scientific and were used without further purification. Solvents were purified by passage through a solvent column composed of activated alumina and a supported copper redox catalyst. All reactions were performed under an atmosphere of dry argon. A Biotage® Initiator microwave system was used for microwave-assisted deprotection. Thin-layer chromatography was carried out

on Silicycle precoated silica gel 60 F254 plates. An Agilent 971-FP flash purification system with various SiliaSep™ (Silicycle, 40-63µm, 60Å) prepacked silica gel cartridges was used for flash column chromatography. ¹H NMR and ¹³C NMR spectra were recorded in the indicated solvent on a Bruker Avance-III (500 MHz and 126 MHz for ¹H and ¹³C, respectively) spectrometer. Chemical shifts are reported as δ values in parts per million downfield from TMS (δ 0.0) as the internal standard in CDCl₃. MS was performed on a system consisting of an electrospray ionization (ESI) source in a Bruker amaZon SL mass spectrometer. High-resolution mass spectra were obtained using an Agilent 6210 LC-TOF spectrometer. The purity of the compounds was evaluated on a Beckman Gold reverse phase analytical HPLC system using an Phenomenex Gemini C-18 (4.6 × 250 mm, 5 µm) or Luna C-8 (4.6 × 250 mm, 5 µm) reverse phase columns with UV absorbance (254 nm). Purities of all compounds that were subjected to biological assay were > 95%.

General procedure for coupling reaction of aryl bromide with lithiated pyrrolyl-lutidine.

Method A

To a solution of **7** (1.2 g, 6.0 mmol) in THF (25 mL) was added n-BuLi (1.6 M solution in hexanes, 3.75 mL, 6.0 mmol), and the reaction was stirred for 30 min at 0 °C. This mixture was transferred to a solution of aryl bromide **8**, **11a-b**, or **15a-c** (5.0 mmol) in THF (25 mL) at -78 °C via cannula. The reaction mixture was allowed to stir for an additional 20 min and then quenched with H₂O (50 mL). After addition of ethyl acetate (50 mL), the organic layer was partitioned, dried with MgSO₄, and concentrated by rotary evaporation. The residue was purified by flash chromatography (EtOAc/hexanes) to yield products **9**, **12a-b**, **16a-c**, respectively.

2-(2,5-Dimethyl-1*H*-pyrrol-1-yl)-6-(3-iodophenethyl)-4-methylpyridine (**9**)

The title compound was prepared using general method A from 3-iodobenzylbromide (**8**). 94%; colorless oil; ¹H NMR (500 MHz, CDCl₃) δ 7.57 – 7.51 (m, 2H), 7.17 (dt, *J* = 7.7, 1.3 Hz, 1H), 7.02 (t, *J* = 7.9 Hz, 1H), 6.91 (s, 1H), 6.89 (s, 1H), 5.92 (s, 2H), 3.06 (m, 4H), 2.40 (s, 3H), 2.15 (s, 6H); ¹³C NMR (126 MHz, CDCl₃) δ 160.35, 151.69, 149.52, 143.95, 137.59, 135.03, 130.11, 128.48, 127.77, 122.70, 120.22, 106.71, 94.40, 39.45, 35.27, 21.02, 13.29; MS ESI [M + H]⁺ = 417.5.

2-(2-(6-Bromopyridin-2-yl)ethyl)-6-(2,5-dimethyl-1*H*-pyrrol-1-yl)-4-methylpyridine (**12a**)

The title compound was prepared using general method A from 2-bromo-6-(bromomethyl)pyridine (**11a**). 91%; colorless oil; ¹H NMR (500 MHz, CDCl₃) δ 7.43 (t, *J* = 7.6 Hz, 1H), 7.32 (d, *J* = 7.9 Hz, 1H), 7.09 (d, *J* = 7.2 Hz, 1H), 7.00 (s, 1H), 6.87 (s, 1H), 5.91 (s, 2H), 3.35 – 3.10 (m, 4H), 2.39 (s, 3H), 2.13 (s, 6H); ¹³C NMR (126 MHz, CDCl₃) δ 162.82, 160.32, 151.58, 149.56, 141.57, 138.65, 128.47, 125.51, 122.80, 121.85, 120.20, 106.65, 37.30, 37.27, 21.01, 13.25; MS ESI [M + H]⁺ = 370.3.

2-(2-(5-Bromopyridin-3-yl)ethyl)-6-(2,5-dimethyl-1*H*-pyrrol-1-yl)-4-methylpyridine (**12b**)

The title compound was prepared using general method A from 3-bromo-5-(bromomethyl)pyridine (**11b**). 89%; colorless oil; ¹H NMR (500 MHz, CDCl₃) δ 8.52 (d, *J* = 2.2 Hz, 1H), 8.34 (d, *J* = 1.9 Hz, 1H), 7.65 (t, *J* = 2.1 Hz, 1H), 6.91 (dt, *J* = 4.0, 1.2 Hz,

2H), 5.92 (s, 2H), 3.24 – 3.00 (m, 4H), 2.40 (s, 3H), 2.14 (s, 6H); ^{13}C NMR (126 MHz, CDCl_3) δ 159.46, 151.83, 149.79, 148.58, 148.08, 138.65, 138.61, 128.45, 122.79, 120.56, 120.51, 106.79, 38.80, 32.12, 21.01, 13.27; MS ESI $[\text{M} + \text{H}]^+ = 370.5$.

2-(3-Bromo-5-(trifluoromethyl)phenethyl)-6-(2,5-dimethyl-1H-pyrrol-1-yl)-4-methylpyridine (16a)

The title compound was prepared using general method A from 3-bromo-5-trifluoromethylbenzylbromide (**15a**). 81%; colorless oil; ^1H NMR (500 MHz, CDCl_3) δ 7.61 (s, 1H), 7.53 (s, 1H), 7.33 (s, 1H), 6.92 (s, 1H), 6.91 (s, 1H), 5.94 (s, 2H), 3.35 – 3.03 (m, 4H), 2.40 (s, 3H), 2.16 (s, 6H); ^{13}C NMR (126 MHz, CDCl_3) δ 159.59, 151.84, 149.79, 144.69, 135.05, 132.22 (q, $J = 32.7$ Hz), 128.48, 126.11 (d, $J = 3.8$ Hz), 124.15 (d, $J = 3.5$ Hz), 123.17 (q, $J = 272.8$ Hz), 122.85, 122.59, 120.49, 106.81, 39.03, 35.02, 20.97, 13.24; MS ESI $[\text{M} + \text{H}]^+ = 437.2$.

2-(3-Bromo-5-fluorophenethyl)-6-(2,5-dimethyl-1H-pyrrol-1-yl)-4-methylpyridine (16b)

The title compound was prepared using general method A from 3-bromo-5-fluorobenzylbromide (**15b**). 81%; pale yellow oil; ^1H NMR (500 MHz, CDCl_3) δ 7.15 (s, 1H), 7.10 (dt, $J = 8.2, 2.1$ Hz, 1H), 6.95 (s, 1H), 6.92 (s, 1H), 6.87 (m, 1H), 5.94 (s, 2H), 3.16 – 3.03 (m, 4H), 2.42 (s, 3H), 2.17 (s, 6H); ^{13}C NMR (126 MHz, CDCl_3) δ 162.60 (d, $J = 250.1$ Hz), 159.89, 151.75, 149.71, 145.63 (d, $J = 7.8$ Hz), 128.46, 127.56 (d, $J = 3.0$ Hz), 122.74, 122.29 (d, $J = 10.2$ Hz), 120.40, 116.69 (d, $J = 24.4$ Hz), 114.42 (d, $J = 20.9$ Hz), 106.79, 38.98, 35.04 (d, $J = 1.8$ Hz), 21.01, 13.28; MS ESI $[\text{M} + \text{H}]^+ = 387.2$.

2-(3,5-Dibromophenethyl)-6-(2,5-dimethyl-1H-pyrrol-1-yl)-4-methylpyridine (16c)

The title compound was prepared using general method A from 3,5-dibromobenzylbromide (**15c**). 86%; pale yellow oil; ^1H NMR (500 MHz, CDCl_3) δ 7.51 (s, 1H), 7.29 (s, 1H), 7.26 (ss, 2H), 6.91 (s, 2H), 5.92 (s, 2H), 3.06 (q, $J = 2.8$ Hz, 4H), 2.40 (d, $J = 1.6$ Hz, 3H), 2.15 (s, 6H); ^{13}C NMR (126 MHz, CDCl_3) δ 159.76, 151.73, 149.72, 145.43, 131.65, 130.43, 128.48, 122.77, 122.74, 120.42, 106.76, 39.02, 34.89, 21.01, 13.27; MS ESI $[\text{M} + \text{H}]^+ = 449.2$.

3-Bromo-5-(2-(6-(2,5-dimethyl-1H-pyrrol-1-yl)-4-methylpyridin-2-yl)ethyl)benzonitrile (17)

A mixture of **16c** (448 mg, 1.0 mmol), CuCN (108 mg, 1.20 mmol), and DMF (4 mL) was heated at 220 °C for 20 min in the microwave cavity. Then the reaction mixture was treated with dichloromethane (20 mL), filtered, and concentrated in *vacuo*. The residue was purified by flash chromatography to give the title compound (225 mg, 57%) as a pale yellow oil. ^1H NMR (500 MHz, CDCl_3) δ 7.63 (s, 1H), 7.57 (s, 1H), 7.41 (s, 1H), 6.93 (ss, 2H), 5.92 (s, 2H), 3.19–3.03 (m, 4H), 2.41 (s, 3H), 2.13 (s, 6H). ^{13}C NMR (126 MHz, CDCl_3) δ 159.27, 151.82, 149.88, 145.04, 136.39, 132.31, 130.76, 128.44, 122.77, 122.75, 120.59, 117.45, 113.92, 106.81, 38.69, 34.58, 21.01, 13.26; MS ESI $[\text{M} + \text{H}]^+ = 394.5$.

General procedure for Buchwald reaction and pyrrole deprotection²⁹ for 10a-d; Method B

To a 5 mL microwave vial equipped with a magnetic stir bar was added aryl iodide **9** (0.5 mmol), an amine (1.0 mmol), $\text{Pd}_2(\text{dba})_3$ (23 mg, 0.025 mmol), DavePhos (20 mg, 0.050

mmol), NaOtBu (58 mg, 0.60 mmol) in THF (1.5 mL) and 1,4-dioxane (1.5 mL). After being purged with dry argon, the reaction mixture were stirred for 5~10 h at 100 °C (oil bath). After being cooled to room temperature, the reaction mixture was passed through a silica gel pad (2 cm), washed with MeOH (10 mL), and concentrated in *vacuo*. After the residue was placed in a 5 mL microwave vial equipped with a magnetic stir bar, ethanol (2.5 mL) and concentrated hydrochloric acid (0.5 mL) were added. The vial was shaken vigorously and then heated in the microwave irradiator for 20 min at 120 °C (as recorded via the IR sensor of the microwave instrument). After being cooled to room temperature, the reaction mixture was concentrated in *vacuo* and purified by flash column chromatography using a SiliaSep™ C18 flash cartridge (25 g, 40-63 μm / 230-400 mesh, Pore Size 60 Å) with 5-80% MeOH in water as the mobile phase.

***N*¹-(3-(2-(6-Amino-4-methylpyridin-2-yl)ethyl)phenyl)-*N*¹,*N*²-dimethylethane-1,2-diamine (10a)**

The title compound (64 mg, 43%) was prepared according to general method B using *N,N'*-dimethylethane-1,2-diamine (88 mg, 1.0 mmol); pale yellow gel; ¹H NMR (500 MHz, MeOD) δ 7.19 (dd, *J* = 8.3, 7.5 Hz, 1H), 6.87 (s, 1H), 6.77 – 6.74 (m, 1H), 6.68 – 6.63 (m, 3H), 3.64 (t, *J* = 6.4 Hz, 2H), 3.27 (t, *J* = 6.4 Hz, 2H), 3.05 – 2.99 (m, 4H), 2.97 (s, 3H), 2.78 (s, 3H), 2.36 (s, 3H); ¹³C NMR (126 MHz, MeOD) δ 159.07, 155.72, 151.15, 150.27, 142.17, 130.57, 119.35, 115.07, 113.12, 110.67, 50.68, 47.95, 39.20, 36.31, 35.93, 34.08, 21.95; HRMS (ESI): calcd for C₁₈H₂₇N₄ [M + H]⁺, 299.2230; found, 299.2236.

***N*¹-(3-(2-(6-Amino-4-methylpyridin-2-yl)ethyl)phenyl)-*N*²,*N*²-dimethylethane-1,2-diamine (10b)**

The title compound (72 mg, 48%) was prepared according to general method B using *N,N*-dimethylethane-1,2-diamine (88 mg, 1.0 mmol); pale yellow gel; ¹H NMR (500 MHz, MeOD) δ 7.10 (t, *J* = 7.8 Hz, 1H), 6.70 (s, 1H), 6.66 (s, 1H), 6.64 – 6.56 (m, 3H), 3.55 (t, *J* = 6.0 Hz, 2H), 3.40 (t, *J* = 6.0 Hz, 2H), 3.06 – 2.98 (m, 4H), 2.96 (s, 6H), 2.35 (s, 3H); ¹³C NMR (126 MHz, MeOD) δ 159.00, 155.73, 150.29, 149.42, 142.11, 130.53, 119.19, 115.00, 114.22, 112.68, 110.66, 57.76, 43.73, 39.83, 36.11, 35.75, 21.95; HRMS (ESI): calcd for C₁₈H₂₇N₄ [M + H]⁺, 299.2230; found, 299.2234.

***N*¹-(3-(2-(6-Amino-4-methylpyridin-2-yl)ethyl)phenyl)-*N*¹-methylethane-1,2-diamine (10c)**

The title compound (49 mg, 35%) was prepared according to general method B using *N*¹-Boc-*N*²-methylethane-1,2-diamine (174 mg, 1.0 mmol); brown gel; ¹H NMR (500 MHz, MeOD) δ 7.14 (t, *J* = 7.8 Hz, 1H), 6.77 (s, 1H), 6.70 – 6.64 (m, 3H), 6.62 (s, 1H), 3.52 (t, *J* = 6.0 Hz, 2H), 3.27 (t, *J* = 6.0 Hz, 2H), 3.04 – 2.94 (m, 4H), 2.77 (s, 3H), 2.36 (s, 3H); ¹³C NMR (126 MHz, MeOD) δ 159.03, 155.74, 150.20, 148.40, 142.25, 130.62, 120.16, 115.05, 115.00, 113.46, 110.70, 49.25, 41.72, 36.04, 35.68, 33.74, 21.95; HRMS (ESI): calcd for C₁₇H₂₅N₄ [M + H]⁺, 285.2074; found, 285.2070.

***N*¹-(3-(2-(6-Amino-4-methylpyridin-2-yl)ethyl)phenyl)-*N*¹-methylpropane-1,3-diamine (10d)**

The title compound (46 mg, 31%) was prepared according to general method B using *N*-Boc-*N*¹-methylpropane-1,3-diamine (188 mg, 1.0 mmol); pale yellow gel; ¹H NMR (500

MHz, MeOD) δ 7.09 (t, J = 7.8 Hz, 1H), 6.69 – 6.64 (m, 2H), 6.62 – 6.55 (m, 3H), 3.27 (t, J = 6.8 Hz, 2H), 3.19 – 3.10 (m, 2H), 3.01 (m, 2H), 2.95 (m, 2H), 2.73 (s, 3H), 2.36 (d, J = 0.9 Hz, 3H), 2.03 (m, 2H); ^{13}C NMR (126 MHz, MeOD) δ 158.98, 155.72, 150.46, 150.10, 141.87, 130.39, 118.38, 115.16, 114.18, 112.41, 110.67, 48.76, 41.82, 36.15, 35.86, 33.82, 26.92, 21.98; HRMS (ESI): calcd for $\text{C}_{18}\text{H}_{27}\text{N}_4$ [M + H] $^+$, 299.2230; found, 229.2227.

General procedure for Buchwald reaction of an amine with an arylhalide; Method C

To a 5 mL microwave vial equipped with a magnetic stir bar was added an aryl halide (**12a-b**, **16a-b**, or **17**, 0.5 mmol), an amine (1.0 mmol), $\text{Pd}_2(\text{dba})_3$ (23 mg, 0.025 mmol), DavePhos (20 mg, 0.050 mmol), NaOtBu (58 mg, 0.60 mmol) in THF (1.5 mL) and 1,4-dioxane (1.5 mL). After being purged with dry argon, the reaction mixture were stirred for 5~10 h at 100 °C (oil bath). The reaction mixture was treated with dichloromethane (20 mL), filtered, and concentrated in *vacuo*. The residue was purified by flash chromatography (dichloromethane/MeOH) to give the corresponding product.

N^1 -(6-(2-(6-(2,5-Dimethyl-1H-pyrrol-1-yl)-4-methylpyridin-2-yl)ethyl)pyridin-2-yl)- N^2 -dimethylethane-1,2-diamine (**13a**)

The title compound (172 mg, 91%) was prepared according to general method C using **12a** (185 mg, 0.5 mmol) and N,N' -dimethylethane-1,2-diamine (88 mg, 1.0 mmol); pale yellow oil; ^1H NMR (500 MHz, MeOD) δ 7.45 (dd, J = 8.5, 7.3 Hz, 1H), 7.30 (s, 1H), 7.03 (s, 1H), 6.53 (dd, J = 11.7, 7.9 Hz, 2H), 5.83 (s, 2H), 3.91 – 3.83 (m, 2H), 3.45 – 3.38 (m, 1H), 3.25 (dd, J = 5.9, 4.8 Hz, 2H), 3.21 – 3.15 (m, 2H), 3.06 (s, 3H), 2.76 – 2.72 (m, 1H), 2.71 (s, 3H), 2.46 (s, 3H), 2.01 (s, 6H); ^{13}C NMR (126 MHz, MeOD) δ 162.66, 160.36, 159.67, 153.03, 152.54, 139.58, 129.44, 124.64, 122.37, 113.28, 107.70, 105.17, 50.81, 45.03, 39.18, 38.11, 37.28, 34.29, 20.96, 13.06; MS ESI [M + H] $^+$ = 378.0.

N^1 -(5-(2-(6-(2,5-Dimethyl-1H-pyrrol-1-yl)-4-methylpyridin-2-yl)ethyl)pyridin-3-yl)- N^2 -dimethylethane-1,2-diamine (**13b**)

The title compound (164 mg, 87%) was prepared according to general method C using **12b** (185 mg, 0.5 mmol) and N,N' -dimethylethane-1,2-diamine (88 mg, 1.0 mmol); pale yellow gel; ^1H NMR (500 MHz, CDCl_3) δ 8.18 (d, J = 2.8 Hz, 1H), 7.84 – 7.72 (m, 1H), 7.15 – 6.97 (m, 2H), 6.88 (s, 1H), 5.87 (s, 2H), 3.89 (t, J = 6.9 Hz, 2H), 3.24 (t, J = 6.9 Hz, 2H), 3.16 – 3.03 (m, 2H), 3.03 – 2.97 (m, 2H), 2.96 (s, 3H), 2.75 (s, 3H), 2.40 (s, 3H), 2.08 (s, 6H); ^{13}C NMR (126 MHz, CDCl_3) δ 160.16, 151.48, 150.05, 144.95, 137.98, 136.68, 131.67, 128.40, 122.93, 120.46, 106.72, 53.49, 48.45, 46.25, 39.05, 38.32, 33.55, 32.92, 21.05, 13.22; MS ESI [M + H] $^+$ = 378.5.

N^1 -(3-(2-(6-(2,5-Dimethyl-1H-pyrrol-1-yl)-4-methylpyridin-2-yl)ethyl)-5-(trifluoromethyl)phenyl)- N^2 -dimethylethane-1,2-diamine (**18a**)

The title compound (180 mg, 75%) was prepared according to general method C using **17a** (219 mg, 0.5 mmol) and N,N' -dimethylethane-1,2-diamine (88 mg, 1.0 mmol); pale yellow oil; ^1H NMR (500 MHz, CDCl_3) δ 7.04 (s, 1H), 7.00 (s, 1H), 6.88 (s, 1H), 6.77 (s, 1H), 6.75 (s, 1H), 5.87 (s, 2H), 3.87 (t, J = 7.1 Hz, 2H), 3.18 – 3.11 (m, 2H), 3.10 – 3.03 (m, 4H), 3.01 (s, 3H), 2.63 (s, 3H), 2.39 (s, 3H), 2.07 (s, 6H); ^{13}C NMR (126 MHz, CDCl_3) δ 160.74,

151.37, 149.98, 148.88, 143.49, 131.44 (q, $J = 31.3$ Hz), 128.47, 124.35 (d, $J = 273.5$ Hz), 123.05, 120.41, 116.09, 114.33 (d, $J = 3.9$ Hz), 106.88 (d, $J = 4.1$ Hz), 106.67, 48.84, 46.24, 39.36, 39.00, 36.08, 33.55, 20.99, 13.10; ESI $[M + H]^+ = 445.1$.

N^1 -(3-(2-(6-(2,5-Dimethyl-1*H*-pyrrol-1-yl)-4-methylpyridin-2-yl)ethyl)-5-fluorophenyl)- N^1,N^2 -dimethylethane-1,2-diamine (18b)

The title compound (160 mg, 80%) was prepared according to general method C using **17** (193mg, 0.5 mmol) and N,N' -dimethylethane-1,2-diamine (88 mg, 1.0 mmol); pale yellow oil; ^1H NMR (500 MHz, CDCl_3) δ 7.01 – 6.95 (m, 1H), 6.92 – 6.86 (m, 1H), 6.36 (dd, $J = 2.3, 1.3$ Hz, 1H), 6.32 – 6.24 (m, 2H), 5.91 (s, 2H), 3.46 (t, $J = 6.6$ Hz, 2H), 3.11 – 3.05 (m, 2H), 3.03 – 2.98 (m, 2H), 2.94 (s, 3H), 2.81 (t, $J = 6.5$ Hz, 2H), 2.50 (s, 3H), 2.40 (s, 3H), 2.15 (s, 6H); ^{13}C NMR (126 MHz, CDCl_3) δ 164.15 (d, $J = 241.5$ Hz), 160.87, 151.61, 150.97 (d, $J = 11.3$ Hz), 149.52, 144.30 (d, $J = 9.6$ Hz), 128.48, 122.65, 120.10, 107.93, 106.70, 103.08 (d, $J = 21.5$ Hz), 96.99 (d, $J = 26.1$ Hz), 52.54, 49.12, 39.59, 38.85, 36.49, 36.30, 21.02, 13.25; MS ESI $[M + H]^+ = 395.2$.

3-(2-(6-(2,5-Dimethyl-1*H*-pyrrol-1-yl)-4-methylpyridin-2-yl)ethyl)-5-(methyl(2-(methylamino)ethyl)amino)benzotrile (18c)

The title compound (145 mg, 72%) was prepared according to general method C using **17** (197 mg, 0.5 mmol) and N,N' -dimethylethane-1,2-diamine (88 mg, 1.0 mmol); colorless gel; ^1H NMR (500 MHz, MeOD) δ 7.22 (s, 1H), 7.01 (s, 1H), 6.95 (s, 1H), 6.91 (s, 1H), 6.83 (s, 1H), 5.82 (s, 2H), 3.57 (t, $J = 6.8$ Hz, 2H), 3.13 – 3.06 (m, 2H), 3.06 – 3.00 (m, 2H), 2.98 (s, 3H), 2.97 – 2.92 (m, 2H), 2.58 (s, 3H), 2.44 (s, 3H), 2.02 (s, 6H); ^{13}C NMR (126 MHz, MeOD) δ 161.95, 152.83, 152.78, 150.99, 145.02, 129.42, 124.79, 122.41, 121.36, 120.54, 118.38, 114.18, 113.79, 107.63, 51.32, 48.45, 39.86, 38.89, 37.05, 35.29, 20.94, 13.13; MS ESI $[M + H]^+ = 402.3$.

General procedure for deprotection of 2-(2,5-dimethyl-1*H*-pyrrol-1-yl)pyridine derivatives using microwave irradiation; Method D

To a 5 mL microwave vial equipped with a magnetic stir bar was added the protected aminopyridine (0.5 mmol), hydroxylamine HCl (173.75 mg), ethanol (2 mL), and water (1 mL). After being capped, the vial was shaken vigorously and then heated in the microwave irradiator for 30 min at 120 °C. The reaction mixture was concentrated in *vacuo*, and purified by flash column chromatography using a SiliaSep™ C18 flash cartridge (25g, 40-63 μm / 230-400 mesh, Pore Size 60 Å) with 5 to 80% MeOH in water as the mobile phase. This method applied to give the products in 62% - 81% yields.

N^1 -(6-(2-(6-Amino-4-methylpyridin-2-yl)ethyl)pyridin-2-yl)- N^1,N^2 -dimethylethane-1,2-diamine (14a)

The title compound (97 mg, 65%) was prepared according to general method D; pale yellow gel; ^1H NMR (500 MHz, MeOD) δ 8.37 (s, 2H), 7.53 – 7.45 (m, 1H), 6.58 (s, 1H), 6.57 (s, 1H), 6.55 (s, 2H), 3.91 (q, $J = 5.6$ Hz, 2H), 3.31 (d, $J = 5.5$ Hz, 2H), 3.07 (s, 3H), 3.05 – 2.98 (m, 4H), 2.77 (s, 3H), 2.32 (s, 3H); ^{13}C NMR (126 MHz, MeOD) δ 160.30, 158.78, 157.34, 157.02, 152.23, 139.68, 114.39, 113.10, 110.20, 105.39, 50.22, 47.99, 38.11, 37.07,

34.37, 34.23, 21.73; HRMS (ESI): calcd for C₁₇H₂₆N₅ [M + H]⁺, 300.2183; found, 300.2189.

N¹-(5-(2-(6-Amino-4-methylpyridin-2-yl)ethyl)pyridin-3-yl)-N¹,N²-dimethylethane-1,2-diamine (14b)

The title compound (105 mg, 70%) was prepared according to general method D; pale brown gel; ¹H NMR (500 MHz, MeOD) δ 8.22 (s, 2H), 8.10 (s, 1H), 6.78 (s, 1H), 6.71 (s, 1H), 3.93 (t, *J* = 6.9 Hz, 2H), 3.39 – 3.35 (m, 2H), 3.29 – 3.22 (m, 2H), 3.20 (s, 3H), 3.19 – 3.14 (m, 2H), 2.81 (s, 3H), 2.40 (s, 3H); ¹³C NMR (126 MHz, MeOD) δ 159.18, 155.84, 148.79, 148.67, 141.90, 129.47, 128.91, 124.88, 115.15, 111.28, 46.78, 38.92, 34.62, 34.12, 32.77, 21.99; HRMS (ESI): calcd for C₁₇H₂₆N₅ [M + H]⁺, 300.2183; found, 300.2188.

N¹-(3-(2-(6-Amino-4-methylpyridin-2-yl)ethyl)-5-(trifluoromethyl)phenyl)-N¹,N²-dimethylethane-1,2-diamine (19a)

The title compound (148 mg, 81%) was prepared according to general method D; colorless gel; ¹H NMR (500 MHz, MeOD) δ 7.22 (s, 1H), 6.91 (s, 1H), 6.89 (s, 1H), 6.69 (ss, 2H), 3.77 (t, *J* = 6.7 Hz, 2H), 3.30 (t, *J* = 6.7 Hz, 2H), 3.09 (d, *J* = 3.1 Hz, 4H), 3.05 (s, 3H), 2.80 (s, 3H), 2.37 (s, 3H); ¹³C NMR (126 MHz, MeOD) δ 159.07, 155.75, 151.14, 149.78, 143.60, 132.76 (q, *J* = 31.3 Hz), 126.96 (q, *J* = 271.8 Hz), 117.77, 115.17, 115.03 (d, *J* = 4.0 Hz), 110.85, 108.46 (d, *J* = 4.0 Hz), 50.12, 47.60, 38.98, 36.13, 35.75, 34.16, 21.99; HRMS (ESI): calcd for C₁₉H₂₅F₃N₄ [M + H]⁺, 367.2104; found, 367.2111.

N¹-(3-(2-(6-Amino-4-methylpyridin-2-yl)ethyl)-5-fluorophenyl)-N¹,N²-dimethylethane-1,2-diamine (19b)

The title compound (120 mg, 76%) was prepared according to general method D; colorless gel; ¹H NMR (500 MHz, MeOD) δ 6.73 (s, 1H), 6.70 (s, 1H), 6.67 (s, 1H), 6.45 (dt, *J* = 12.5, 2.3 Hz, 1H), 6.40 (dt, *J* = 9.3, 1.6 Hz, 1H), 3.72 (t, *J* = 6.7 Hz, 2H), 3.26 (t, *J* = 6.7 Hz, 2H), 3.07 – 3.00 (m, 4H), 2.99 (s, 3H), 2.78 (s, 3H), 2.36 (s, 3H); ¹³C NMR (126 MHz, MeOD) δ 165.55 (d, *J* = 241.2 Hz), 159.03, 155.76, 152.21 (d, *J* = 11.0 Hz), 149.92, 144.33 (d, *J* = 9.7 Hz), 115.09, 110.83, 110.28, 105.19 (d, *J* = 22.1 Hz), 99.28 (d, *J* = 26.6 Hz), 50.22, 47.60, 39.16, 36.16, 35.65, 34.15, 22.05; HRMS (ESI): calcd for C₁₈H₂₅FN₄ [M + H]⁺, 317.2136; found, 317.2142.

3-(2-(6-Amino-4-methylpyridin-2-yl)ethyl)-5-(methyl(2-(methylamino)ethyl)amino)benzotrile (19c)

The title compound (100 mg, 62%) was prepared according to general method D; pale yellow gel; ¹H NMR (500 MHz, MeOD) δ 7.22 (s, 1H), 7.02 (s, 1H), 6.98 (s, 1H), 6.68 (ss, 2H), 3.73 (t, *J* = 6.7 Hz, 2H), 3.27 (t, *J* = 6.7 Hz, 2H), 3.12 – 3.05 (m, 4H), 3.04 (s, 3H), 2.79 (s, 3H), 2.38 (s, 3H); ¹³C NMR (126 MHz, MeOD) δ 159.11, 155.80, 151.08, 149.67, 143.98, 121.71, 120.26, 118.78, 115.03, 114.97, 114.23, 110.89, 49.93, 47.50, 38.85, 35.79, 35.48, 34.10, 21.95; HRMS (ESI): calcd for C₁₉H₂₆N₅ [M + H]⁺, 324.2183; found, 324.2187.

Oxyhemoglobin assays

The oxyhemoglobin NO assays were performed with purified NOSs using a Biotek Gen5™ microplate reader as previously reported.^{27,28} The following were included in the assay: 10 μM L-arginine, 100 μM NADPH, 10 μM tetrahydrobiopterin, 1 mM CaCl₂, 11.6 μg/mL calmodulin, 3.0 μM oxyhemoglobin, and 100 mM HEPES buffer (10% glycerol; pH 7.4). For iNOS, calmodulin and CaCl₂ were omitted because iNOS is calcium independent. All NOS isozymes were used at a concentration of approximately 100 nM. IC₅₀ for each compound was determined in triplicate using dose-response curves with nine concentration points (1 pM - 3 mM). The calculated standard deviations of the assays were less than 10% with all NOSs. The inhibition constants (K_i) were calculated from the IC₅₀ and K_m (human nNOS: 1.6 μM; rat nNOS: 1.3 μM; murine iNOS = 8.2 μM; bovine eNOS = 1.7 μM) for all NOSs using the general equation: $K_i = IC_{50} / (1 + [S] / K_m)$. The selectivity of antagonism of nNOS was determined by calculating the ratios of the K_i values with iNOS or eNOS to those with rat nNOS.

Pharmacokinetic study

A group of forty-eight male mice were divided into two groups: Group 1 (2 mg/kg; i.v.) and Group 2 (10 mg/kg; p.o.) with each group comprising twenty-four mice. Animals in Group 1 were administered intravenously with a **19c** solution in saline at a 2 mg/kg dose, and animals in Group 2 were administered orally with a 10 mg/kg solution of **19c** in saline. Blood samples (approximately 100 μL) were collected from the retro orbital plexus under light isoflurane anesthesia; samples were obtained at 0.08, 0.25, 0.5, 1, 2, 4, 8 and 24 h (i.v.) and 0.25, 0.5, 1, 2, 4, 6, 8 and 24 h (p.o.). The blood samples were collected from a set of three mice at each time point in labeled micro centrifuge tubes containing K₂EDTA as anticoagulant. Plasma samples were separated by centrifugation of whole blood and stored below -70 °C until bioanalysis. Immediately after collection of blood, brain samples were collected from each mouse at 0.08, 0.25, 0.5, 1, 2, 4, 8 and 24 h (i.v.) and 0.25, 0.5, 1, 2, 4, 6, 8 and 24 h (p.o.). Tissue samples were homogenized using ice-cold phosphate buffer saline (pH 7.4) and homogenates were stored below -70 °C until analyzed. The total homogenate volume was three times that of the tissue weight. All samples were processed for analysis by protein precipitation using acetonitrile (ACN) and analyzed with a fit for purpose LC/MS/MS method (LLOQ: 2.02 ng/mL for plasma and 3.03 ng/g for brain). Specific LC-MS/MS and MRM conditions are described in the Supporting Information. Pharmacokinetic parameters were calculated using the non-compartmental analysis tool of Phoenix WinNonlin (Version 6.3).

Inhibitor Complex Crystal Preparation

The preparations of rat nNOS, bovine eNOS, and human nNOS heme domains used for crystallographic studies were carried out using the procedures described previously.²³ The heme domain samples of rat nNOS (at 9 mg/mL containing 20 mM histidine) and bovine eNOS (10 mg/mL containing 2 mM imidazole) were used for the sitting drop vapor diffusion crystallization setup under conditions reported.^{22,23} Human nNOS crystals were obtained with the triple K301R/R354A/G357D mutant heme domain sample at 10 mg/mL. By slightly modifying the original conditions^{22,23} where the monoclinic C2 crystals grew, a

new crystal form was obtained. Long plate crystals were grown at 4 °C with the sitting drop setup against a well solution of 8-9% PEG3350, 40 mM citric acid, 60 mM Bis-Tris-Propane, pH 6.2, 10% glycerol, and 5 mM TCEP. New crystals belong to the orthorhombic $P2_12_12_1$ space group with cell dimensions of $a = 52.3 \text{ \AA}$ $b = 122.7 \text{ \AA}$ $c = 165.0 \text{ \AA}$ with one homodimer in the asymmetric unit, which closely resemble the cell dimensions of rat nNOS crystal. Fresh crystals were first passed stepwise through cryoprotectant solutions and then soaked with 10 mM inhibitor for 4-6 h at 4 °C before being flash cooled with liquid nitrogen.

X-ray Diffraction Data Collection, Data Processing, and Structural Refinement

The cryogenic (100 K) X-ray diffraction data were collected remotely at the Stanford Synchrotron Radiation Lightsource (SSRL) or Advanced Light Source (ALS) using the data collection control software Blu-Ice³⁰ with a crystal mounting robot. When a Q315r CCD detector was used, 90-100° of data were typically collected with 0.5° per frame. If a Pilatus pixel array detector was used, 140-160° of fine-sliced data were collected with 0.2° per frame. Raw CCD data frames were indexed, integrated, and scaled using HKL2000³¹ or MOSFLM,³² but the pixel array data were processed with XDS³³ and scaled with Scala (Aimless).³⁴ The binding of inhibitors was detected by the initial difference Fourier maps calculated with REFMAC.³⁵ The inhibitor molecules were then modeled in COOT³⁶ and refined using REFMAC or PHENIX.³⁷ Water molecules were added in REFMAC or PHENIX and checked manually in COOT. The TLS³⁸ protocol was implemented in the final stage of refinements with each subunit as one TLS group. The omit $F_o - F_c$ density maps were calculated by removing inhibitor coordinates from the input PDB file before running one more round of TLS refinement in REFMAC or in PHENIX (simulated annealing protocol with a 2000 K initial temperature). The resulting map coefficients DELFTW and PHDELWT were used to generate maps. The refined structures were validated in COOT before deposition in the protein data bank. The crystallographic data collection and structure refinement statistics are summarized in Table S1 of the Supporting Information, with the PDB accession codes included.

Supplementary Material

Refer to Web version on PubMed Central for supplementary material.

ACKNOWLEDGMENTS

The authors are grateful for financial support from the National Institutes of Health (GM049725 to R.B.S. and GM057353 to T.L.P.). We thank Dr. Bettie Sue Siler Masters (NIH grant GM52419, with whose laboratory P.M. and L.J.R. are affiliated). B.S.S.M. also acknowledges the Welch Foundation for a Robert A. Welch Distinguished Professorship in Chemistry (AQ0012). P.M. is supported by grants 0021620806 and 1M0520 from MSMT of the Czech Republic. We also thank the beamline staff at SSRL and ALS for their assistance during the remote X-ray diffraction data collections.

ABBREVIATIONS

NO	nitric oxide
nNOS	neuronal nitric oxide synthase

iNOS	inducible nitric oxide synthase
eNOS	endothelial nitric oxide synthase
L-Arg	L-arginine
FAD	flavin adenine dinucleotide
FMN	flavin mononucleotide
NADPH	reduced nicotinamide adenine dinucleotide phosphate
H4B	(6 <i>R</i>)-5,6,7,8-tetrahydrobiopterin

REFERENCES

- (1). Garthwaite J, Boulton CL. Nitric oxide signaling in the central nervous system. *Annu. Rev. Physiol.* 1995; 57:683–706. [PubMed: 7539993]
- (2). Garcia-Cardena, Guillermo; Oh, P.; Liu, J.; Schnitzer, JE.; Sessa, WC. Targeting of nitric oxide synthase to endothelial cell caveolae via palmitoylation: implications for nitric oxide signaling. *Proc. Natl. Acad. Sci.* 1996; 93:6448–6453. [PubMed: 8692835]
- (3). Alderton WK, Cooper CE, Knowles RG. Nitric oxide synthases: structure, function and inhibition. *Biochem. J.* 2001; 357:593–615. Pt 3. [PubMed: 11463332]
- (4). Knowles RG, Moncada S. Nitric oxide synthases in mammals. *Biochem. J.* 1994; 298:249–258. [PubMed: 7510950]
- (5). Titheradge MA. Nitric oxide in septic shock. *Biochim. Biophys. Acta, Bioenerg.* 1991; 1411:437–455.
- (6). Morris BJ, Markus A, Glenn CL, Adams DJ, Colagiuri S, Wang L. Association of a functional inducible nitric oxide synthase promoter variant with complications in type 2 diabetes. *J. Mol. Med. (Heidelberg, Ger.)*. 2002; 80:96–104.
- (7). Dorheim MA, Tracey WR, Pollock JS, Grammas P. Nitric oxide synthase activity is elevated in brain microvessels in Alzheimer's disease. *Biochem. Biophys. Res. Commun.* 1994; 205:659–665. [PubMed: 7528015]
- (8). Giasson BI, Duda JE, Murray IV, Chen Q, Souza JM, Hurtig HI, Ischiropoulos H, Trojanowski JQ, Lee VM. Oxidative damage linked to neurodegeneration by selective alpha-synuclein nitration in synucleinopathy lesions. *Science*. 2000; 290:985–989. [PubMed: 11062131]
- (9). Norris PJ, Waldvogel HJ, Faull RL, Love DR, Emson PC. Decreased neuronal nitric oxide synthase messenger RNA and somatostatin messenger RNA in the striatum of Huntington's disease. *Neuroscience*. 1996; 72:1037–1047. [PubMed: 8735228]
- (10). Huang PL, Huang Z, Mashimo H, Bloch KD, Moskowitz M, A, Bevan JA, Fishman MC. Hypertension in mice lacking the gene for endothelial nitric oxide synthase. *Nature*. 1995; 377:239–242. [PubMed: 7545787]
- (11). Lassen HL, Iversen HK, Olesen J. A dose_response study of nitric oxide synthase inhibition in different vascular beds in man. *Eur. J. Clin. Pharmacol.* 2003; 59:499–505. [PubMed: 13680036]
- (12). Ramnauth J, Renton P, Dove P, Annedi SC, Speed J, Silverman S, Mladenova J, Maddaford SP, Zinghini S, Rakhit S, Andrews J, Lee DK, Zhang D, Porreca F. Discovery of dual inducible/neuronal nitric oxide synthase (iNOS/nNOS) inhibitor development candidate 4-((2-Cyclobutyl-1*H*-imidazo[4,5-*b*]pyrazin-1-yl)methyl)-7,8-difluoroquinolin-2(1*H*)-one (KD7332) Part 2: Identification of a novel, potent, and selective series of benzimidazole-quinolinone iNOS/nNOS dimerization inhibitors that are orally active in pain models. *J. Med. Chem.* 2012; 55:2882–2893. [PubMed: 22335555]
- (13). Ramnauth J, Speed J, Maddaford SP, Subhash C, Renton AP, Rakhit S, Andrews J, Silverman S, Mladenova G, Zinghini S, Nair N, Catalano C, Lee D, Felice MD, Porreca F. Design, synthesis, and biological evaluation of 3,4-Dihydroquinolin-2(1*H*)-one and 1,2,3,4-Tetrahydroquinoline-

- based selective human neuronal nitric oxide synthase (nNOS) inhibitors. *J. Med. Chem.* 2011; 54:5562–5575. [PubMed: 21699209]
- (14). Annedi SC, Ramnauth J, Maddaford SP, Renton P, Rakhit S, Mladenova G, Dove P, Silverman S, Andrews JS, Felice MD, Porreca F. Discovery of *cis-N*-(1-(4-(Methylamino)cyclohexyl)indolin-6-yl)thiophene-2-carboximidamide: A 1,6-disubstituted indoline derivative as a highly selective inhibitor of human neuronal nitric oxide synthase (nNOS) without any cardiovascular liabilities. *J. Med. Chem.* 2012; 55:943–955. [PubMed: 22175766]
- (15). Ji H, Delker SL, Li H, Martásek P, Roman LJ, Poulos TL, Silverman RB. Exploration of the active site of neuronal nitric oxide synthase by the design and synthesis of pyrrolidinomethyl 2-aminopyridine derivatives. *J. Med. Chem.* 2010; 53:7804–7824. [PubMed: 20958055]
- (16). Kang S, Tang W, Li H, Chreifi G, Martásek P, Roman LJ, Poulos TL, Silverman RB. Nitric oxide synthase inhibitors that interact with both heme propionate and H₄B show high isoform selectivity. *J. Med. Chem.* 2014; 57:4382–4396. [PubMed: 24758147]
- (17). Cinelli MA, Li H, Chreifi G, Martásek P, Roman LJ, Poulos TL, Silverman RB. Simplified 2-aminoquinoline-based scaffold for potent and selective neuronal nitric oxide synthase inhibition. *J. Med. Chem.* 2014; 57:1513–1530. [PubMed: 24472039]
- (18). Mukherjee P, Li H, Sevrioukova I, Chreifi G, Martásek P, Roman LJ, Poulos TL, Silverman RB. Novel 2,4-disubstituted pyrimidines as potent, selective, and cell-permeable inhibitors of neuronal nitric oxide synthase. *J. Med. Chem.* 2015; 58:1067–1088. [PubMed: 25489882]
- (19). Mukherjee P, Cinelli MA, Kang S, Silverman RB. Development of nitric oxide synthase inhibitors for neurodegeneration and neuropathic pain. *Chem. Soc. Rev.* 2014; 43:6814–6838. [PubMed: 24549364]
- (20). (a) Hagmann WK, Caldwell CG, Chen P, Durette PL, Esser CK, Lanza TJ, Kopka IE, Guthikonda R, Shah SK, MacCoss M, Chabin RM, Fletcher D, Grant SK, Green BG, Humes JL, Kelly TM, Luell S, Meurer R, Moore V, Pacholok SG, Pavia T, Williams HR, Wong KK. Substituted 2-aminopyridines as inhibitors of nitric oxide synthases. *Bioorg. Med. Chem. Lett.* 2000; 10:1975–1978. [PubMed: 10987430] (b) Lowe JA III, Qian W, Volkmann RA, Heck S, Nowakowski J, Nelson R, Nolan C, Liston D, Ward K, Zorn S, Johnson C, Vanase M, Faraci WS, Verdries KA, Baxter J, Doran S, Sanders M, Ashton M, Whittle P, Stefaniak M. A new class of selective and potent inhibitors of neuronal nitric oxide synthase. *Bioorg. Med. Chem. Lett.* 1999; 9:2569–2572. [PubMed: 10498210] (c) Lowe JA III, Qian W, Drozda SE, Volkmann RA, Nason D, Nelson RB, Nolan C, Liston D, Ward K, Faraci S, Verdries K, Seymour P, Majchrzak M, Villalobos A, White WF. Structure-activity relationships of potent, selective inhibitors of neuronal nitric oxide synthase based on the 6-phenyl-2-aminopyridine structure. *J. Med. Chem.* 2004; 47:1575–1586. [PubMed: 14998342]
- (21). Fedorov R, Vasana R, Ghosh DK, Schlichting I. Structures of nitric oxide synthase isoforms complexed with the inhibitor AR-R17477 suggest a rational basis for specificity and inhibitor design. *Proc. Natl. Acad. Sci.* 2004; 101:5892–5897. [PubMed: 15071192]
- (22). Li H, Jamal J, Delker S, Plaza C, Ji H, Jing Q, Huang H, Kang S, Silverman RB, Poulos TL. The mobility of a conserved tyrosine residue controls isoform-dependent enzyme-inhibitor interactions in nitric oxide synthases. *Biochemistry.* 2014; 53:5272–5279. [PubMed: 25089924]
- (23). Li H, Jamal J, Plaza C, Pineda SH, Chreifi G, Jing Q, Cinelli MA, Silverman RB, Poulos TL. Structures of human constitutive nitric oxide Synthases. *Acta Crystallogr.* 2014; D70:2667–2674.
- (24). (a) Huang H, Li H, Yang S, Chreifi G, Martásek P, Roman LJ, Meyskens FL, Poulos TL, Silverman RB. Potent and selective double-headed thiophene-2-carboximidamide inhibitors of neuronal nitric oxide synthase for the treatment of melanoma. *J. Med. Chem.* 2014; 57:686–700. [PubMed: 24447275] (b) Jing Q, Li H, Roman LJ, Martásek P, Poulos TL, Silverman RB. Combination of chiral linkers with thiophenecarboximidamide heads to improve the selectivity of inhibitors of neuronal nitric oxide synthase. *Bioorg. Med. Chem. Lett.* 2014; 24:4504–4510. [PubMed: 25149509]
- (25). Huang H, Li H, Martásek P, Roman LJ, Poulos PL, Silverman RB. Structure-guided design of selective inhibitors of neuronal nitric oxide synthase. *J. Med. Chem.* 2013; 56:3024–3032. [PubMed: 23451760]

- (26). Surry DS, Buchwald SL. Dialkylbiaryl phosphines in Pd-catalyzed amination: a user's guide. *Chem. Sci.* 2011; 2:27–50. [PubMed: 22432049]
- (27). Labby KJ, Xue F, Kraus JM, Ji H, Mataka J, Li H, Martásek P, Roman LJ, Poulos TL, Silverman RB. Intramolecular hydrogen bonding: A potential strategy for more bioavailable inhibitors of neuronal nitric oxide synthase. *Bioorg. Med. Chem.* 2012; 20:2435–2443. [PubMed: 22370337]
- (28). Hevel JM, Marletta MA. Nitric-oxide synthase assays. *Methods Enzymol.* 1994; 233:250–258. [PubMed: 7516999]
- (29). Walia A, Kang S, Silverman RB. Microwave-assisted protection of primary amines as 2,5-dimethylpyrroles and their orthogonal deprotection. *J. Org. Chem.* 2013; 78:10931–10937. [PubMed: 24073706]
- (30). McPhillips TM, McPhillips SE, Chiu HJ, Cohen AE, Deacon AM, Ellis PJ, Garman E, Gonzalez A, Sauter NK, Phizackerley RP, Soltis SM, Kuhn P. Blu-Ice and the Distributed Control System: software for data acquisition and instrument control at macromolecular crystallography beamlines. *J. Synchrotron Radiat.* 2002; 9:401–406. [PubMed: 12409628]
- (31). Otwinowski Z, Minor W. Processing of X-ray diffraction data collected in oscillation mode. *Methods Enzymol.* 1997; 276:307–326.
- (32). Leslie, AGW.; Powell, HR.; Read, JR.; Sussman, JL. *Evolving Methods for Macromolecular Crystallography*; Springer; Dordrecht, The Netherlands: 2007. Processing diffraction data with Mosflm; p. 41-51.
- (33). Kabsch W. XDS. *Acta Crystallogr.* 2010; D66:125–132.
- (34). Evans PR. Scaling and assessment of data quality. *Acta Crystallogr.* 2006; D62:72–82.
- (35). Murshudov GN, Vagin AA, Dodson EJ. Refinement of macromolecular structures by the maximum-likelihood method. *Acta Crystallogr.* 1997; D53:240–255.
- (36). Emsley P, Cowtan K. Coot: model-building tools for molecular graphics. *Acta Crystallogr.* 2004; D60:2126–2132.
- (37). Adams PD, Afonine PV, Bunkóczi G, Chen VB, Davis IW, Echols N, Headd JJ, Hung L-W, Kapral GJ, Grosse-Kunstleve RW, McCoy AJ, Moriarty NW, Oeffner R, Read RJ, Richardson DC, Richardson JS, Terwilliger TC, Zwart PH. PHENIX: a comprehensive Python-based system for macromolecular structure solution. *Acta Crystallogr.* 2010; D66:213–221.
- (38). Winn MD, Isupov MN, Murshudov GN. Use of TLS parameters to model anisotropic displacements in macromolecular refinement. *Acta Crystallogr.* 2001; D57:122–133.

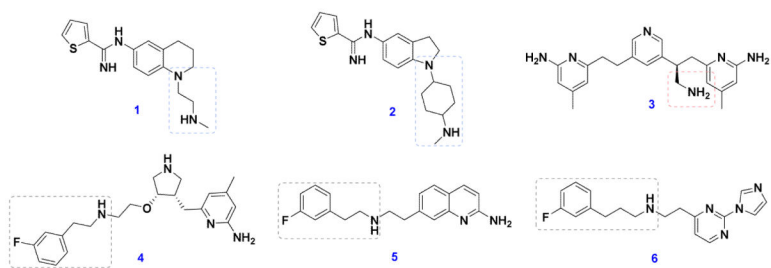


Figure 1.
Structures of recent nNOS inhibitors, which share common pharmacophores

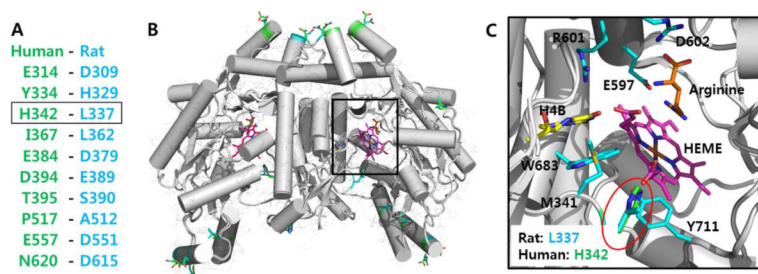


Figure 2.

Crystal structure overlays of rat (PDB:1OM4, cyan) and human (PDB:4D1N, green) nNOS heme domains. Nonidentical pairs within the heme domain are summarized in (A) and highlighted with side chains shown in (B) and identical sequences shown as a gray cartoon, heme in pink, and arginine in orange. (C) zoom-in view of the substrate (arginine) binding site, where the only nonidentical pair H342 (human) – L337(rat) is located near Y711 (red circle). All structural figures were prepared with PyMol (www.pymol.org).

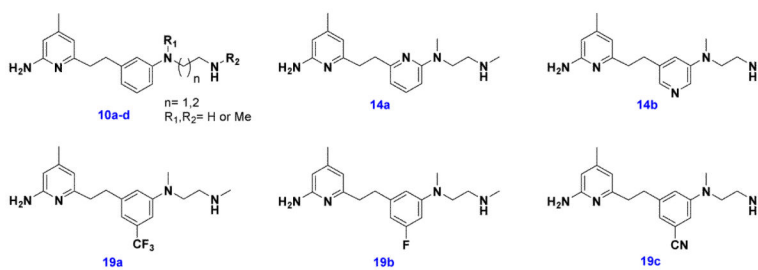


Figure 3. Structures of synthesized N^1, N^2 -dimethylethylenediamine derivatives reported in this study

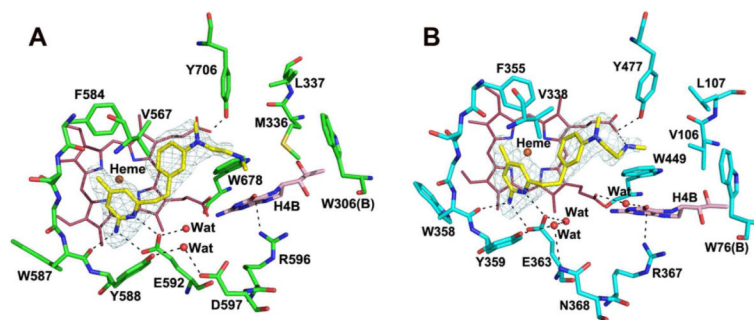


Figure 4. Structure of compound **10a** bound to nNOS (A) or eNOS (B). The omit Fo – Fc electron density for the inhibitor is shown at the 2.5 σ contour level. Major hydrogen bonds are depicted with dashed lines.

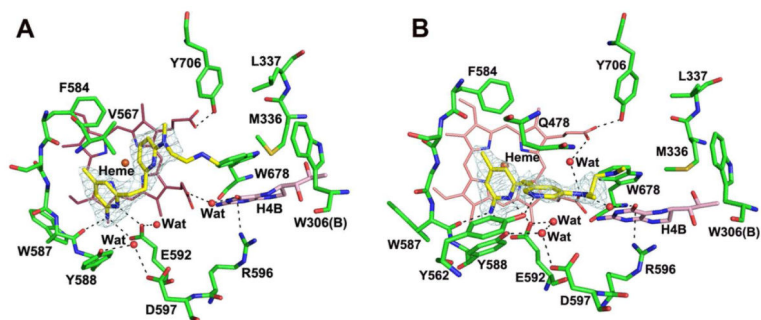


Figure 5. Active site structure of nNOS with either **14a** (A) or **14b** (B) bound. The omit Fo – Fc electron density for the inhibitor is shown at the 2.5 σ contour level. Major hydrogen bonds are depicted with dashed lines.

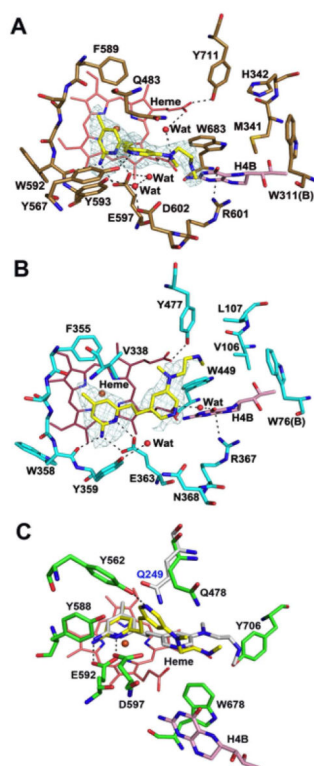


Figure 6. Active site structure of human nNOS (**A**) or bovine eNOS (**B**) with **14b** bound. The omit $F_o - F_c$ electron density for the inhibitor is shown at the 2.5σ contour level. Major hydrogen bonds are depicted with dashed lines.

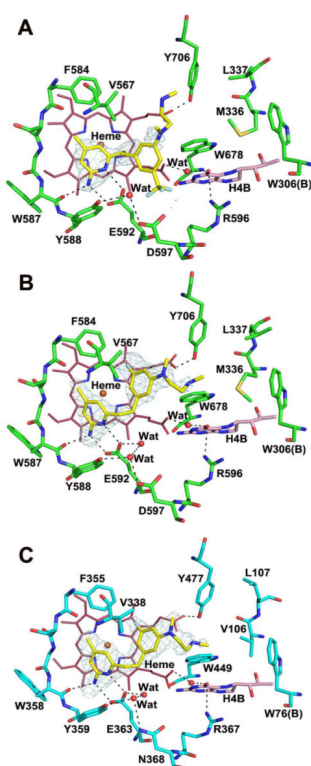


Figure 7. Active site structures of (A) rat nNOS with **19a**, (B) rat nNOS with **19b**, and (C) bovine eNOS with **19b** bound. The omit Fo – Fc electron density for the inhibitor is shown at the 2.5 σ contour level. Major hydrogen bonds are depicted with dashed lines.

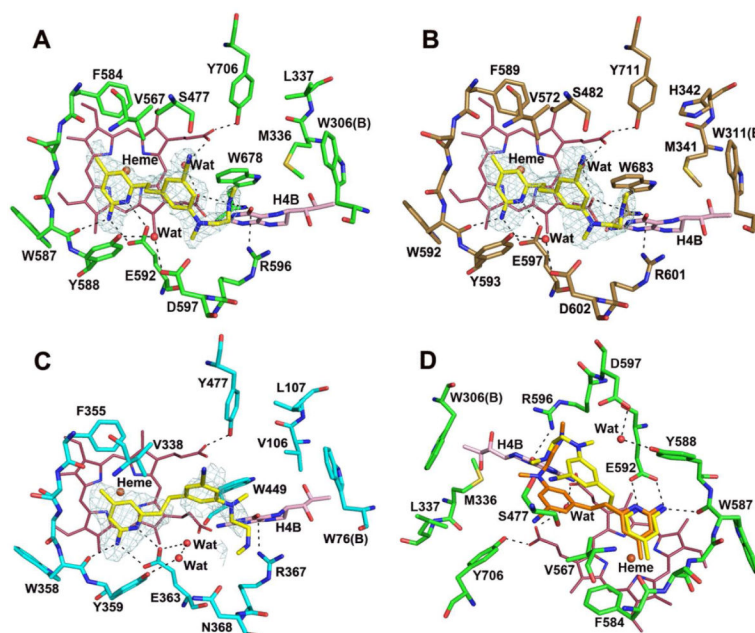
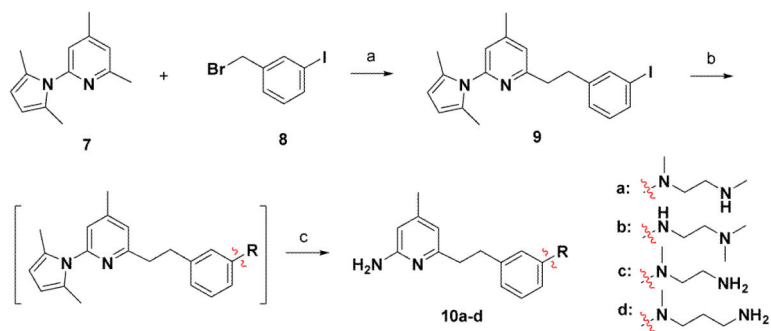
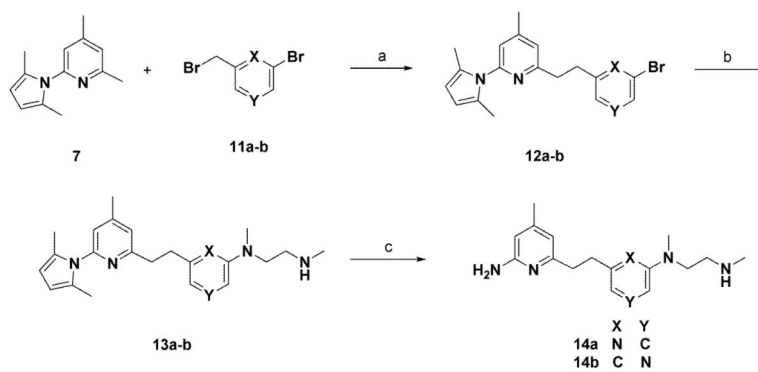


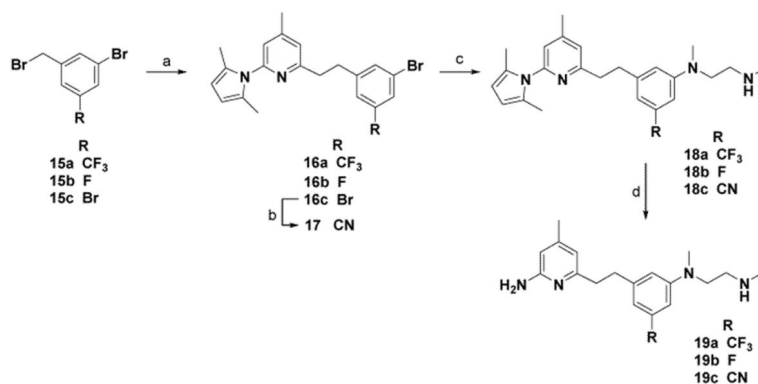
Figure 8. Active site structures of rat nNOS (A), human nNOS (B), and bovine eNOS (C) with **19c** bound. The omit $F_o - F_c$ electron density for the inhibitor is shown at the 2.5σ contour level. Major hydrogen bonds are depicted with dashed lines. (D) The superimposition of two **19c** positions found in rat nNOS and bovine eNOS. The view is flipped from that in panel (A) in order to clearly show two different conformations of **19c** in nNOS (yellow) and eNOS (orange).

**Scheme 1^a**

^aReagents and conditions: (a) (i) **7**, BuLi, 0 °C, 30 min, THF; (ii) **8**, 94%; (b) Pd₂(dba)₃, DavePhos, NaOtBu, diamine a-d, THF, 1,4-dioxane, 5~10 h, 100 °C; (c) conc-HCl, EtOH, microwave, 120 °C, 20 min. two-step yield: 31-48%.

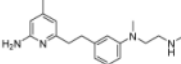
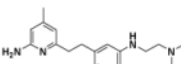
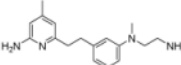
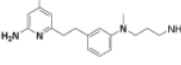
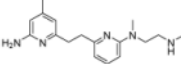
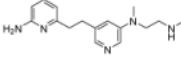
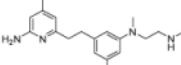
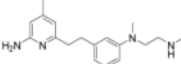
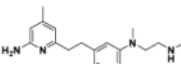
**Scheme 2^a**

^aReagents and conditions: (a) (i) **7**, BuLi, 0 °C, 30 min, THF; (ii) **11a-b**, 89-91%; (b) *N*¹,*N*²-dimethylethane-1,2-diamine (2 equiv), Pd₂(dba)₃, DavePhos, NaOtBu, THF, 1,4-dioxane, 5~10 h, 100 °C, 87-91%; (c) NH₂OH·HCl (5 equiv), EtOH, H₂O, microwave, 120 °C, 30 min, 65-70%.

**Scheme 3^a**

^aReagents and conditions: (a) (i) **7**, BuLi, 0 °C, 30 min, THF; (ii) **15a-c**, 81-86%; (b) CuCN, DMF, microwave, 220 °C, 20 min, 57%; (c) *N*¹,*N*²-dimethylethane-1,2-diamine (2 equiv), Pd₂(dba)₃, DavePhos, NaO*t*Bu, THF, 1,4-dioxane, 5 h, 100 °C, 75%; (d) NH₂OHC1 (5 equiv), EtOH, H₂O, microwave, 120 °C, 30 min, 62-81%.

Table 1List of K_i values and selectivity

Name	structure	K_i (nM) [*]				i/n	e/n
		Rat nNOS	H nNOS	iNOS	eNOS		
10a		130 ± 10	98 ± 5	5,340 ± 336	20,240 ± 1032	41	156
10b		190 ± 12	111 ± 9	5,430 ± 412	23,700 ± 1432	29	125
10c		62 ± 4.1	56 ± 2	2,900 ± 187	10,675 ± 874	47	172
10d		430 ± 22	109 ± 3	4,640 ± 296	10,680 ± 886	11	25
14a		35 ± 2.0	64 ± 2.2	4,845 ± 310	17,742 ± 1244	138	507
14b		17 ± 1.6	59 ± 3.2	2,152 ± 129	12,910 ± 1008	127	759
19a		67 ± 3.3	189 ± 16	8,134 ± 760	15,940 ± 1266	122	238
19b		34 ± 1.2	105 ± 8.1	5,559 ± 421	30,238 ± 2046	166	903
19c		24 ± 1.1	55 ± 3.4	3,669 ± 223	24,950 ± 1684	153	1040

* K_i for each compound was determined in triplicate using dose-response curves with nine concentration points (1 pM - 3 mM). The calculated standard deviations (\pm S.D.) of the assays were less than 10% with all NOSs.

Table 2DMPK data in mice for compound **19c**

route	matrix	T _{max} (hr)	^a C ₀ /C _{max} (ng/mL)	AUC _{last} (hr*ng/mL)	AUC _{inf} (hr*ng/mL)	T _{1/2} (hr)	CL (mL/min/kg)	V _{ss} (L/kg)	%F ^b
i.v.	plasma	-	471.70	180.38	181.00	1.12	184.16	14.75	-
	brain ^c	-	100.28	789.07	NR ^d	24.80	21.18	44.01	
p.o.	plasma	0.25	50.75	162.43	182.46	-	-	-	18%
	brain ^c	4.00	39.31	673.67	NR ^d	-	-	-	

^a back extrapolated conc. for i. v. group.^b AUC_{last} considered for calculating the bioavailability^c Brain concentrations and exposures are expressed as ng/g and h*ng/g, respectively. Density of brain homogenate was considered 1, which is equivalent to the plasma density.^d NR – not reported since AUC_{inf} is 20% greater than AUC_{last}